Available online at www.sciencedirect.com

ScienceDirect

Procedia Engineering 133 (2015) 576 – 589

Procedia Engineering

www.elsevier.com/locate/procedia

6th Fatigue Design Conference, Fatigue Design 2015

Fatigue Behaviour of Additively Manufactured Ti-6Al-4V

Amanda Sterling[a], Nima Shamsaei[a,b]*, Brian Torries[a], Scott M. Thompson[a,b]

[a]*Mississippi State University, Department of Mechanical Engineering, PO Box 9552 Mississippi State, MS, 39762, USA*

[b]*Mississippi State University, Center for Advanced Vehicular Systems (CAVS), PO Box 5405, Mississippi State, MS, 39762, USA*

Abstract

Fatigue behaviour of Ti-6Al-4V specimens additively-manufactured via Laser Engineered Net Shaping (LENS) is investigated in this study. Additive manufacturing provides the opportunity to fabricate complex geometries layer-by-layer from 3D computer aided drawings. As the mechanical behaviour of metallic materials depends on their microstructure, which is affected by the time-temperature history, additive-manufactured components are expected to have different properties than those of their wrought counterparts. Ti-6Al-4V rods were fabricated by LENS using two different sets of process parameters and machined into 'dog-bone' fatigue specimens with dimensions in conformance to ASTM standards. The fatigue behaviour and microstructural features of the LENS Ti-6Al-4V samples were characterized and compared with wrought Ti-6Al-4V. Fractography of the fractured specimen surfaces was performed using Scanning Electron Microscopy (SEM) to determine the failure mechanism and realize the effects of porosity on fatigue resistance and data scatter of LENS Ti-6Al-4V. The fatigue lives of the LENS Ti-6Al-4V materials were found to be lower than those of the wrought Ti-6Al-4V, and driven by the porosity and microstructure of the samples.

Peer-review under responsibility of CETIM

Keywords: Laser Engineered Net Shaping (LENS); Direct Laser Deposition, Fatigue; Ti-6Al-4V; Additive Manufacturing; Defects

1. Introduction

Nomenclature

ε_f	True Fracture Ductility (%)
$\varepsilon`_f$	Fatigue Ductility Coefficient (MPa)
σ_u	True Ultimate Tensile Strength (MPa)
σ_y	True Yield Stress (MPa)
$\sigma`_f$	Fatigue Strength Coefficient (MPa)
b	Fatigue Strength Exponent

Peer-review under responsibility of CETIM
doi:10.1016/j.proeng.2015.12.632

c	Fatigue Ductility Exponent
E`	Cyclic Modulus of Elasticity (GPa)
K`	Cyclic Strength Coefficient (MPa)
n`	Cyclic Strain Hardening Exponent

Titanium alloys are used for many applications across several industries because they possess a desirable combination of material characteristics. The applications of Ti-6Al-4V are numerous and include their use for: aerospace components, bio-implants, automobiles and petrochemical components. Often referred to as the 'workhorse' of the titanium alloys, Ti-6Al-4V is a competitive material that is being investigated for its use via additive manufacturing (AM).

Additive manufacturing is the process of fabricating a part layer-by-layer by utilizing a combination of energy delivery and material deposition. For metallic materials, it is common to use powders that are melted successively using a directed energy source such as a laser or electron beam. The major AM processes for metallic part fabrication include Selective Laser Melting (SLM), a Powder Bed Fusion-Laser (PBF-L) method, and Laser Engineered Net Shaping (LENS), a Directed Energy Deposition (DED) method. For DED methods, metallic powders are blown into a laser beam for combined deposition/energy-delivery. Various DED processes are now demonstrating the potential to generate Ti-6Al-4V parts for direct end-usage in a variety of applications [1]. Via SLM or LENS, parts with complex geometry, unobtainable using traditional manufacturing methods, can be more readily produced - presenting new opportunities in component design. With these unique AM methods, a greater control over material microstructure, and thus mechanical properties, is obtainable by virtue of a process-sensitive thermal history.

Laser Engineered Net Shaping (LENS), as shown in Fig. 1(a), utilizes multiple nozzles to spray powder into a laser beam (typically Nd:YAG). Argon is utilized for purging the LENS chamber to ensure an inert atmosphere for minimizing oxidization during deposition. The LENS method can be broken down into four general steps. The first step involves pumping a laser through the deposition head to create a melt pool on a metal substrate. Spherical, powdered metal is then blown into the melt pool, resulting in a small molten bead. Next, a user-defined tool-path directs the deposition head to move in the desired spatial pattern. Since the laser and blown powder are continually active, this movement will extend that molten bead into a molten line, or track. By overlapping these tracks, a solid, single-layer shape is created. Finally, the deposition head is raised upward by a user-defined layer thickness, and the previous steps are repeated in order to create the next layer. By repeating this process, a solid metallic part is created.

LENS is unique in comparison to PBF-L methods in that multiple axes and powder feeders can be utilized for generating functionally-graded materials or to repair precious components. Since there is no powder bed that surrounds parts fabricated via LENS, the ability to monitor the thermal history of parts can allow for greater design freedom and quality control. For these reasons, among others, LENS Ti-6Al-4V has many opportunities.

Most components will undergo cyclic loading, making fatigue the most likely cause of failure during service. Since fatigue behaviour can be affected by the microstructure of material, the unique thermal history imposed on AM parts is of interest. In fact, the microstructure of AM parts can be highly anisotropic and/or contain features different than traditional wrought materials. One example of this is the columnar grains that grow epitaxially through the deposition layers due to cooling. Epitaxial growth occurs when the tops of these columnar grains are re-melted during the deposition of the next layer. The previously-formed columnar grains may serve as nucleation points for the new grains, and the growth continues [2, 3].

Different sets of LENS process parameters can lead to different microstructures encumbered in the part. For example, increasing the laser power typically results in lower local cooling rates, and therefore, larger microstructures. A mixture of columnar and equiaxed grains, rather than just columnar grains, can also result from increased laser power [4]. Increasing the travel speed (i.e. relative speed between part and laser) usually increases local cooling rates, leading to finer microstructures. Coarse grains can result from increasing the powder feed rate; however, this coarseness decreases as the build progresses [4]. These different microstructures resulting from different parameter sets can lead to different mechanical behaviour [2, 4-7].

Some research into the fatigue properties of AM Ti-6Al-4V has already been initiated. In one study, the high cycle fatigue (HCF) behaviour of DED Ti-6Al-4V specimens was shown to match that of the wrought Ti-6Al-4V. This finding was attributed to the shape of the α-lamellae present in the specimen microstructure; the small width resulted in high yield strength and thus improved HCF strength [8]. Conversely, there have been two fatigue studies conducted on AM Ti-6Al-4V material produced via electron beam AM methods, with fatigue specimens (as-built and machined) fabricated in both horizontal and vertical orientations. None of the results could compete with the wrought part fatigue performance [9, 10].

This current work continues on a previous fatigue study performed by the authors on LENS Ti-6Al-4V [11], where the fatigue life was found to not match that of the wrought material. In this effort, two different LENS Ti-6Al-4V samples were fabricated using two different parameter sets (e.g. powder feed rate, laser power, etc.) in order to establish distinct microstructures. Mechanical behaviour of each LENS sample was compared with that of wrought Ti-6Al-4V material, and the microstructural features for each LENS sample is identified. Monotonic tensile tests, as well as fully reversed, strain controlled fatigue tests, were conducted on the specimens. The resulting monotonic and cyclic properties are discussed and related to the microstructure and process defects. The fracture surfaces were inspected in order to discern the fracture behaviour. Conclusions are drawn from the experimental results and discussion.

2. Experimental program

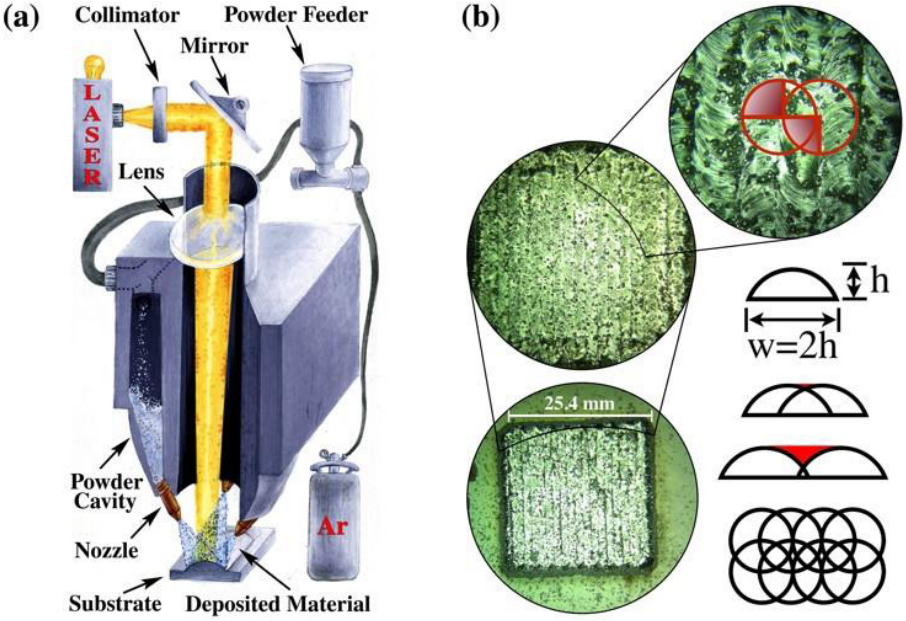

Fig. 1. (a) Representative schematic of LENS process and (b) a visual representation of hatch spacing.

There are many minutiae other than the primary LENS process parameters for successfully generating a part. These include, but are not limited to, the deposition head height, layer thickness, hatch spacing, layer orientation, and powder particle size. If these details are not carefully balanced, then process defects (such as voids) are introduced into the build. The deposition head height has direct bearing on the diameter of the melt pool, which is dependent on tpower input from the laser. The larger the melt pool diameter is, the higher the laser power must be to accommodate the larger surface area. The capability of the actual laser equipment and the sturdiness of the focusing lens must also be taken into account, to insure that the desired melt pool size can be created without damaging any equipment. If the laser power is not high enough, the melt pool will not be sufficient to generate a

full molten bead, and this can result in a poor build containing more porosity and defects.

The diameter of the melt pool ties into the calibration of the hatch spacing. Figure 1(b) illustrates the utilized geometry for the cross section of a molten bead. The width of the semi-circle area should be twice as wide as the height for ensuring successful deposition. Overlapping the molten lines (molten lines being an extended molten bead) by 50% creates an analogue of a flat surface. If proper hatch spacing is ignored, then the "trench" formed in between two molten lines can trap pockets of gas between layers. The height of the molten bead atop the substrate allows one to calibrate for layer thickness during LENS, as well.

Another source for pore generation in LENS parts is the utilization of powder with pre-existing voids. Small pockets of gas are sometimes already trapped in the small metallic particles (residual defects from the manufacturing process), and introduced into the build through no fault of the operator. This is one of the more difficult issues to address during LENS parameter selection.

For the current study, the effect of microstructure and porosity within cylindrical LENS samples on their eventual fatigue behaviour is sought. Hence, one series of samples, i.e. LENS Series 1, was fabricated with induced porosity, in order to characterize the mechanical behaviour that stems from pores. By strategically selecting the LENS process parameters, LENS Series 1 was fabricated with a combination of parameters that produced columnar grains with interspersed prior β-grains, while LENS Series 2 was printed with smaller, more uniformly sized grains. The LENS Series 1 and LENS Series 2 specimens also differed in sample density. Fatigue data was generated for wrought TI-6Al-4V to be used for comparison purposes.

The DED/AM machine used to fabricate the Ti-6Al-4V cylindrical specimens (10.92 mm diameter, 101.60 mm tall) was an OPTOMEC LENS 750, powered by a 1 kW Nd:YAG laser. For building the rods, the building strategy included a 0.02 mm hatch spacing, a 0.02 mm layer thickness, and an alternating layer orientation (0° and 90°). The Ti-6Al-4V powder (-100+325 mesh) was used as-provided and ensured to meet SAE AMS 4998C [12].

After the primary cylinders were created, they were machined down to the traditional 'dogbone' specimens, with dimensions that obey the ASTM E 606-92 standard (7.0 mm grip diameter, 18.0 mm gauge length, and 3.5 mm gauge diameter) [13]. The gage section was polished (sandpapers of progressively finer grit) to a mirror finish. This was done in order to minimize the effects of surface quality on the fatigue results, allowing microstructure and porosity to be the main focus. Small amounts of epoxy were applied to two places on the gauge section, where the tines of an extensometer could be applied without scarring the surface finish. An MTS Tabletop 858 machine was utilized for a series of strain-controlled fully-reversed uniaxial tension-compression fatigue tests, along with an MTS Extensometer (model 634.31F-25).

3. Experimental Results and Discussions

3.1. Microstructure

A comparison of the LENS Series 1 and LENS Series 2 microstructures is shown in Figure 2. It may be seen that the microstructure of the LENS 2 samples differs drastically from that observed in the LENS Series 1 samples. The grains found in the LENS Series 1 samples, seen in Figure 2a, vary in size, with large grains on the exterior and a mixture of large prior β-grains and interwoven laths in the interior. The LENS 2 microstructure, shown in Figure 2b, consists of small grains that are generally uniform in shape and size, lacking the large prior-β grains found in the LENS Series 1 samples. Additionally, the LENS 2 microstructure exhibits very little epitaxial growth, a common feature in the LENS Series 1 microstructure. When etched, it was observed that the α lathes of LENS Series 1 were longer and finer than those found in LENS 2. The wrought microstructure differed from both the LENS Series 1 and Series 2. Rather than columnar grains, it consisted of small, 10 μm diameter equiaxed grains. These differences in microstructure appear to be due to the different thermal histories, and cooling rates, of the samples experienced during fabrication. The unique thermal history inherent to LENS Series 1 samples is observed to have led to larger grains with greater epitaxial growth than the grains within the LENS 2 microstructure. The mill annealing process that the wrought samples underwent most likely led to the smaller, equiaxed grains.

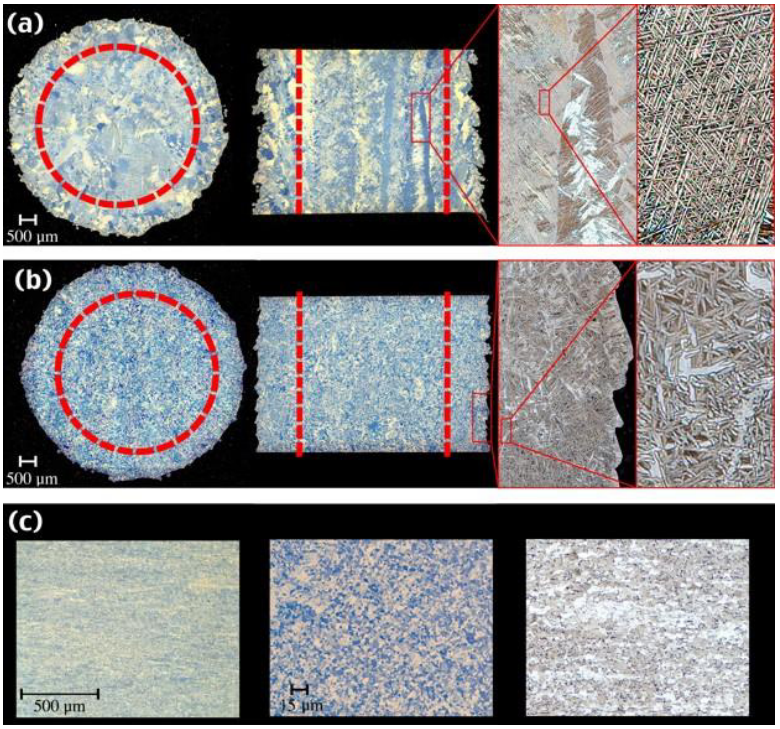

Fig. 2. Microstructure of a cylinder from a) LENS Series 1, b) LENS Series 2, and c) wrought Ti-6Al-4V; Left: Surface in the radial plane. Center: Surface in the longitudinal plane. Right: magnifications depicting surface etched with 2% hydrofluoric acid, 98% water [11].

3.2. Tensile and cyclic deformation

Figure 3 shows a comparison of six monotonic tensile tests, four of which were performed on LENS Ti-6Al-4V fabricated with two different sets of parameters, and the final two performed on wrought Ti-6Al-4V. Table 1 lists their average monotonic properties including monotonic modulus of elasticity, yield stress, ultimate tensile strength (UTS), and fracture ductility.

The wrought material had a higher yield point and UTS than LENS Series 1 material, while the elastic moduli were similar. The LENS Series 1 also demonstrated more scatter in results than the wrought material. Upon examination of the fracture surfaces of the LENS Series 1 specimens, a pattern was apparent. The tougher specimens possessed fewer defects on their fracture surface, as can be seen in Figure 4. It is important to note that Specimen 1, shown in Fig. 4, had a porosity level unique to it only; as none of the other specimens, fatigue or monotonic, exhibited a similar porosity level. As there appears to be a direct relationship between the monotonic tensile behaviour and the presence of process defects, optimizing the LENS process to remove those defects would most likely improve the mechanical behaviour of the material.

The LENS Series 2 Ti-6Al-4V had comparable results to the wrought Ti-6Al-4V. While the true yield stress was slightly lower than the wrought (by 3.9%) and slightly higher than LENS Series 1, the UTS was slightly higher than the wrought (by 1.6%) and higher than the LENS Series 1 (by 6.4%). The elastic modulus of LENS Series 2 was lower than both LENS Series 1 and the wrought Ti-6Al-4V. Overall, the LENS Series 2 Ti-6Al-4V performed better than the LENS Series 1 Ti-6Al-4V, but did have slightly lower fracture ductility.

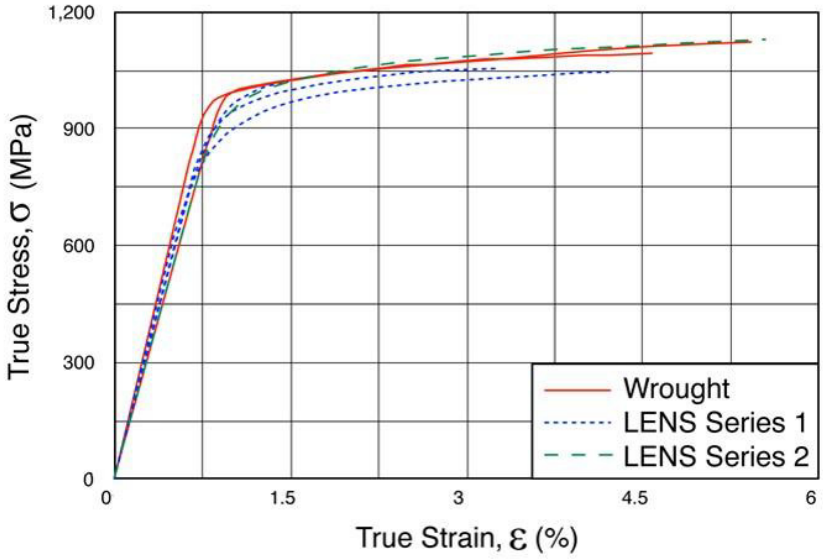

Fig. 3. Tensile stress-strain curves for wrought and LENS Ti-6Al-4V [11].

Table 1. Tensile and cyclic properties of LENS Series 1 [11], LENS Series 2, and wrought specimens.

Tensile Properties	LENS Series 1	LENS Series 2
Monotonic Modulus of Elasticity, E (GPa)	119	108
True Yield Stress, σ_y (MPa)	908	956
True Ultimate Tensile Strength, σ_u (MPa)	1,038	1,126
True Fracture Ductility, ε_f (%)	15.2	13.4
Cyclic Properties		
Cyclic Modulus of Elasticity, E' (GPa)	106	126
Cyclic Strength Coefficient, K' (MPa)	2,145	1,320
Cyclic Strain Hardening Exponent, n'	0.134	0.060
Fatigue Strength Coefficient, σ'_f (MPa)	2,310	2,115
Fatigue Strength Exponent, b	-0.136	-0.127
Fatigue Ductility Coefficient, ε'_f (MPa)	0.256	7.55
Fatigue Ductility Exponent, c	-0.797	-1.290

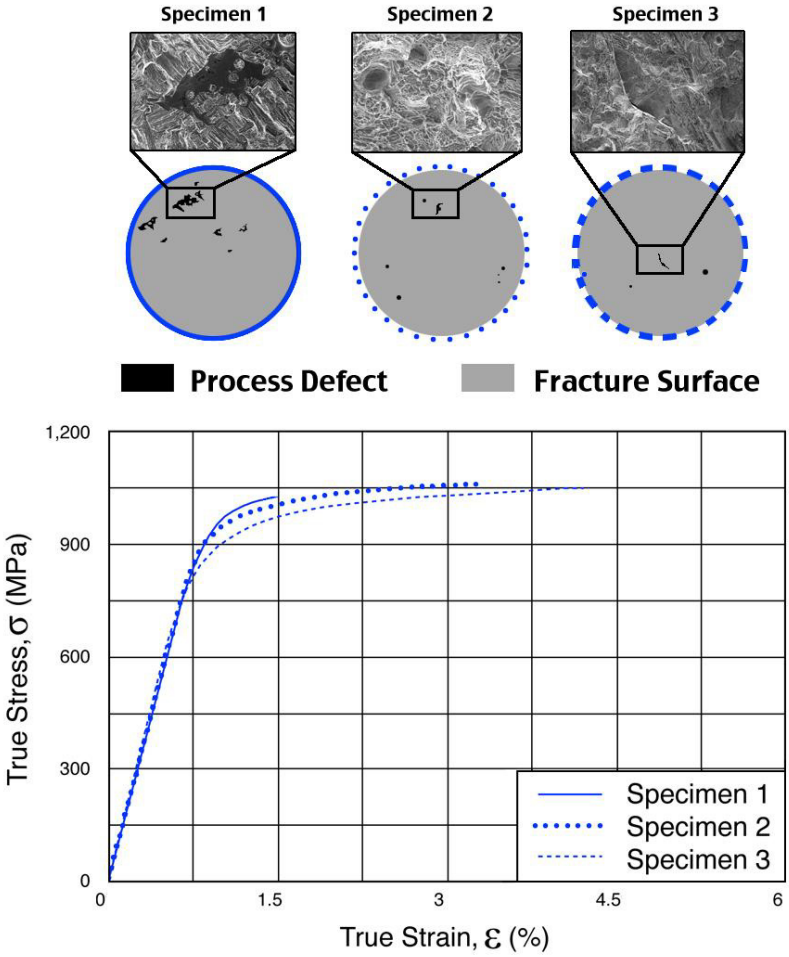

Fig. 4. Comparison of three monotonic tensile tests conducted on three specimens of LENS Series 1 Ti-6Al-4V [11]. The grayscale representations of the fracture surfaces correspond to LENS tensile specimens 1, 2, and 3, from left to right. Grey represents the general fracture surface, while black indicates a process defect, such as voids or areas with lack of fusion.

Figure 5 shows the cyclic stress-strain data and fit (i.e., Ramberg-Osgood curves) superimposed upon the monotonic curves for wrought Ti-6Al-4V and both LENS fabricated series, and Figure 6 compares the Ramberg-Osgood cyclic curves for all three materials. The cyclic deformation properties for the wrought, LENS Series 1, and LENS Series 2 are listed in Table 1. The wrought Ti-6Al-4V experienced cyclic softening overall, while the LENS specimens had no obvious cyclic softening or hardening. As seen from Figure 6, both LENS series had higher stress responses than wrought, therefore, the wrought demonstrates more ductile behaviour.

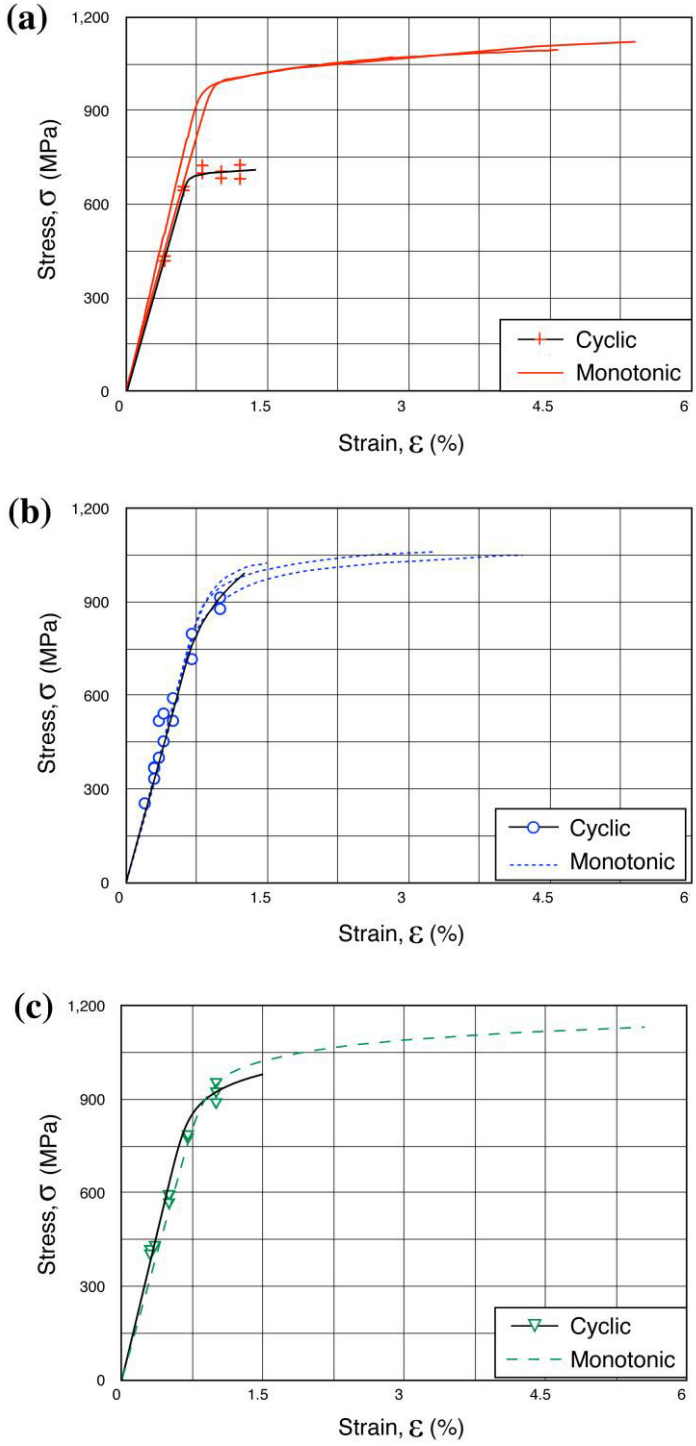

Fig. 5. Comparison of cyclic stress-strain curve (Ramberg-Osgood) and data with the monotonic tensile curves of Ti-6Al-4V for (a) wrought, (b) LENS Series 1 [11], and (c) LENS Series 2.

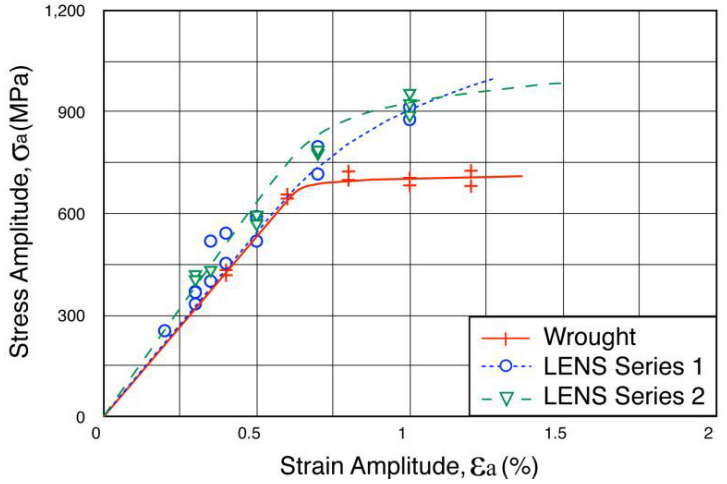

Fig. 6. Comparison of Romberg-Osgood cyclic stress-strain curves for wrought, LENS Series 1 [11], and LENS Series 2 Ti-6Al-4V.

3.3. Fatigue behaviour

Figure 7 displays the fatigue curves generated using the Coffin-Manson approach for both sets of LENS specimens and the wrought material (strain amplitudes that contained runout tests were not included in the Coffin-Manson calculations). Plastic data from lower strain amplitudes was not used in the fit for LENS Series 2, as the values were so small they were considered to be zero. Judging by how little plastic strain is present in either material, the behaviour of both LENS Ti-6Al-4V series is primarily elastic, with noticeable plastic strain occurring at 1% strain amplitude. The wrought Ti-6Al-4V experiences more plastic strain than both LENS materials, with noticeable amounts starting at 0.8% strain amplitude.

Figure 8 compares the fatigue curves for the two LENS Ti-6Al-4V materials and the wrought Ti-6Al-4V. The wrought material performed better than both LENS materials, and the LENS Series 1 material generally did better than the LENS Series 2 material. In the low-cycle regimes of both types of LENS specimens, the materials were penalized due to a lack of ductility, and in the high-cycle regimes, the fatigue was defect-driven. It has been found that the fatigue behaviour of the LENS samples is driven by elastic rather than plastic strain. This can be seen in Figure 7, where the plastic and elastic curves in Figure 7b and 7c do not intersect. After investigation into the fracture surfaces using scanning electron microscopy (SEM), the variation in the data was linked to a noticeable prevalence in voids.

There were two other batches of LENS Ti-6Al-4V in this study that underwent a beta anneal and a heat treatment surpassing the beta transus temperature. These specimens underwent the same machining and fatigue tests [11], however, the results indicate these processes were ineffectual. These results suggest a need for an improved optimization process for LENS Ti-6Al-4V in order to eliminate the porosity inherent to the current process. By accomplishing this, the material behaviour will most likely see a marked improvement.

An investigation of the fatigue specimen fracture surfaces was conducted using SEM and the results are displayed in Figure 9. A 45º angle of the surface initiation site was observed for wrought Ti-6Al-4V specimens. Both crack propagation and final failure zones were very clear, presenting a ‘clean’ and easily readable fracture surface. This was not the case with either of the LENS fabricated materials.

Both LENS materials experienced a more brittle-type failure, as multiple crack initiation sites were observed adjacent to porosity on the facture surfaces. As there can be more than one void, there can be multiple crack initiation sites on a single fracture surface. Both types of fracture surfaces had very mountainous features, often making the crack propagation sites difficult to determine.

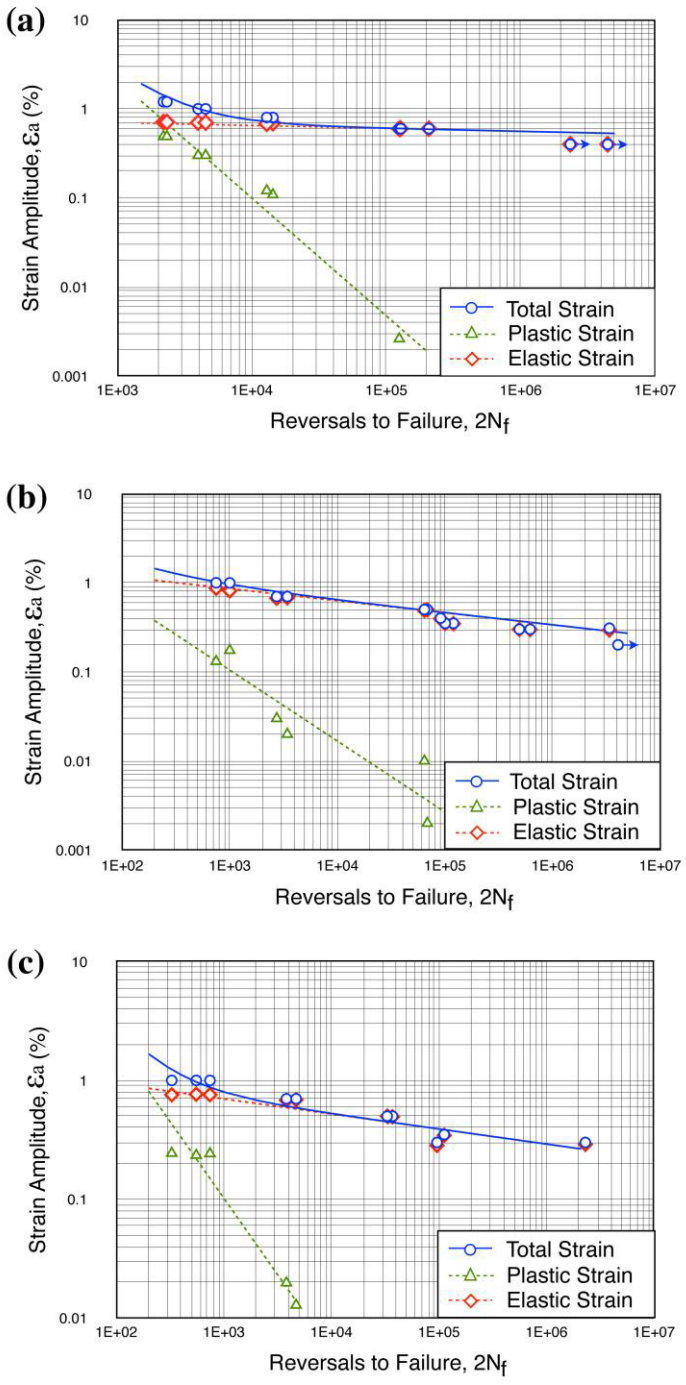

Fig. 7. Total, elastic, and plastic strain plotted against reversals to failure for fully reversed, strain controlled fatigue tests for a) wrought, b) LENS Series 1 [11], and c) LENS Series 2 Ti-6Al-4V.

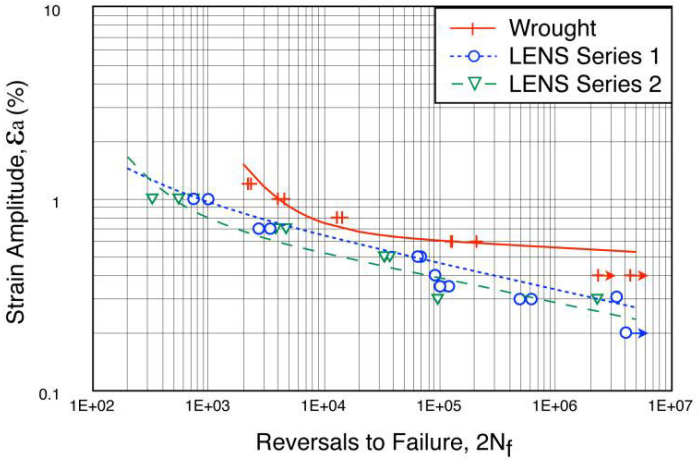

Fig. 8. Strain-life fatigue behaviour of wrought, LENS Series 1 [11], and LENS Series 2 Ti-6Al-4V.

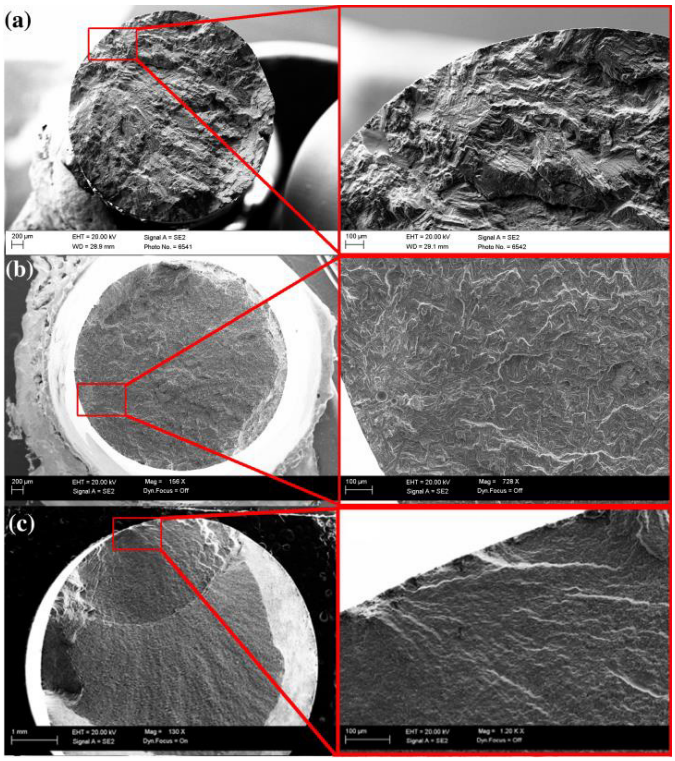

Fig. 9. Representative fracture surfaces for a) LENS Series 1 Ti-6Al-4V [10], b) LENS Series 2 Ti-6Al-4V, c) and wrought Ti-6Al-4V.

A void can exist as gas that becomes trapped in the melt pool during the deposition process. The majority of the voids are spherical, as seen in Figure 10(a). However, there are cases where the shape of the voids are less uniform, due to multiple pockets of gas coalescing or areas experiencing lack of fusion. The one common feature shared between all the voids seen in this study is the smooth interior surface, seen in Figures 10(b) and 10(c).

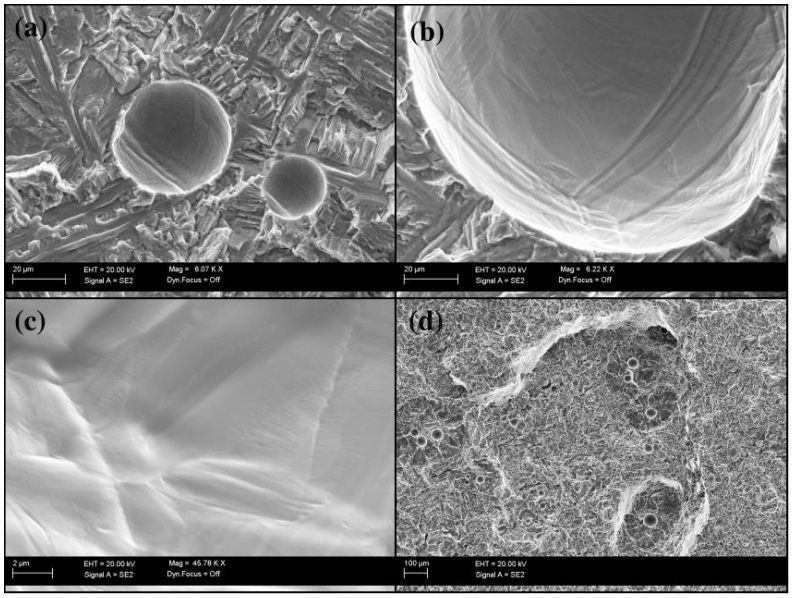

Fig. 10. a) Two typical spherical voids, b) view of interior void wall, c) magnified view of interior void wall, and d) fatigue fracture surface featuring voids with different depths and sizes.

During the fractography investigation of the LENS materials, the number, size, and position of the voids along each fracture surface was documented and compared with the fatigue results. There was found to be a relationship between the fatigue life of a specimen and the presence of porosity. Five main relationships were identified, the first being related to void size: the larger the void, the greater its effect on the fatigue behaviour. The second relationship is that the closer to the surface the void is located; a shorter fatigue life is expected. It was found that the greater number of voids present, the greater the effect on shortening the fatigue lives. The fourth relationship involved the shape of the void: the less uniform the void shape, the greater its effect on fatigue of the part. The non-spherical shapes, particularly those with sharp corners and edges, tend to have stress concentrations that make crack initiation more likely to occur at that site. Finally, in cases involving multiple pores, it was found that the closer together a group of voids are located with respect to each other, the greater their effect on the fatigue behaviour - resulting in shorter fatigue lives.

These relationships were observed in both the LENS Series 1 and Series 2 specimens. However, there were some tests that did not adhere to these relationships. One possible explanation for this deviation could be the crack propagating into, and being temporarily arrested by, a spherical void. Further, a crack could have been forced to travel around a void, deviating from the more direct path and therefore prolonging the crack growth. An example of this can be seen in Figure 10(d), where the crack path can be seen travelling around a group of voids existing at different depths in the sample.

As mentioned earlier, voids existing at different depths in a specimen's gage section can cause cracks to initiate at those differing depths. Eventually, those cracks will propagate and coalesce, having to travel horizontally and vertically through the material. However, porosity is not the only thing to dictate how the crack will propagate. The material's underlying microstructure also plays a large role. For example, the LENS Series 1 material is visually more 'jagged' than the LENS 2 material. This can be explained by existence of beta grain growth in the LENS Series 1 material, and the absence of beta grain growth in the LENS Series 2 material.

Finer microstructures, consisting of more grain boundaries, can lead to lower fatigue life at higher strain amplitudes (i.e., short life regime) since the grain boundaries act as crack nucleation sites [14]. This can be seen in the increased fatigue life at higher strain amplitudes of the LENS Series 1 as compared to the LENS Series 2 specimens. Finer microstructure typically results in longer fatigue lives at lower strain amplitudes; however, the LENS Series 2 specimens, while having finer microstructure than the LENS Series 1 specimens, had shorter fatigue

lives. This could be due to the increased porosity present in the LENS Series 2 samples acting as crack initiation sites and dominating the fatigue behaviour at long life regimes.

5. Conclusions

The often-uncontrollable 'defects' inherent in the LENS process makes it difficult to predict the fatigue behaviour in high cycle regimes for LENS Ti-6Al-4V materials. Voids present in the material can shorten fatigue life by different amounts, depending on the geometry and location of the voids. This results in scatter in the fatigue data. Not only is the fatigue life less predictable than that of wrought Ti-6Al-4V, it is also much shorter. Porosity is perhaps the main culprit, making the need for an effective, LENS parameter optimization procedure clear. This procedure would reduce the porosity, make the fatigue life more predictable, and, ideally, increase the fatigue life to a level comparable to wrought.

In summary, the LENS Ti-6Al-4V materials (i.e. LENS Series 1 and LENS Series 2), each with their own distinct microstructure, were found to have different mechanical properties than the wrought Ti-6Al-4V investigated. It was found that both LENS materials had a lower yield stress than the wrought and that the LENS Series 2 specimens had a higher UTS than the wrought, while the wrought had a higher UTS than LENS Series 1 specimens. In addition, the wrought material had a higher elastic modulus than LENS Series 2, but was similar to that of the LENS Series 1. Of the two LENS Series, LENS Series 2 had a slightly lower elastic modulus and fracture ductility.

Both LENS materials experienced behaviour that was primarily elastic, though the wrought material exhibited noticeable plastic strains at 0.8% and higher strain amplitudes. The wrought material experienced overall cyclic softening, though both LENS materials experienced minor cyclic hardening at strain amplitudes below 1%. At 1% strain amplitude, the LENS materials saw noticeable cyclic softening.

Both LENS Ti-6Al-4V materials had shorter fatigue lives than that of the wrought Ti-6Al-4V; largely due to porosity. Both LENS Ti-6Al-4V materials had fatigue behaviour driven by defects generated during the LENS process. In the high cycle regime, there was more scatter in the data than in the low cycle regime. The shorter lives in the low cycle regimes, however, seemed to be due to a lack of ductility.

Different LENS process parameters can produce different microstructures in the parts manufactured, thus leading to different mechanical properties—fatigue behaviour being one of the more prominent examples. This illustrates a need for a microstructural-sensitive fatigue model that would take these differences into account and predict the fatigue lives of LENS Ti-6Al-4V. This tool could grant the ability to dictate what microstructure is produced in an as-built component for achieving mechanical properties tailored to a specific application. As this study is further developed, monotonic and cyclic data will be collected for a range of microstructures and AM process parameters to calibrate such a model.

References

[1] Bian, L., Thompson, S.M., Shamsaei, N., "Mechanical Properties and Microstructural Features of Direct Laser-Deposited Ti-6Al-4V," JOM, Vol. 67, No. 3, 2015, pp. 629-638.
[2] Wu, Xinhua, et al, "Microstructures of laser-deposited Ti-6Al-4V,"Materials and Design, Vol. 25, No. 2, 2014, pp. 137-144.
[3] Selcuk, C., "Laser metal deposition for powder metallurgy parts," Powder Metallurgy, Vol 54, Issue 2, 2011, pp. 94-99.
[4] Mutombo, K, 2013, "Metallurgical evaluation of laser additive manufactured Ti6Al4V components" Rapid Product Development Association of South Africa (RAPDASA) conference, SanParks Golden Gate Hotel, South Africa.
[5] Pilchak, A.L., Bhattacharjee, A., Williams, R.E.A., Williams, J.C., "The Effect of Microstructure on Fatigue Crack Initiation in Ti-6Al-4V" 2009, International Conference on Fracture (ICF12), Ottawa.
[6] Pilchak, A.L., Nakase, K.I.I., Shirai, Y., Rosenberger, A.H. Williams, J.C., "The Influence on Microstructure and Microtexture on Fatigue crack Initiation and Growth in Alpha + Beta Titanium" 2011, Technical paper: ADA553373, Air Force Research Lab Wright-Patterson AFL, OH.
[7] Rafi, K. H., Karthik, N.V., Starr, Thomas L., Stucker, Brent E. "Mechanical Property Evaluation of Ti-6Al-4V Parts Made Using Electron Beam Melting," Solid Freeform Fabrication Symposium, SFF23, Laboratory for Freeform Fabrication at The University of Texas at Austin, 2012.
[8] Brandl, E., Leyens, C., Palm, F. "Mechanical Properties of Additive Manufactured Ti-6Al-4V using Wire and Powder Based Processes," Trends in Aerospace Manufacturing 2009 International Conference, TRAM09, IOP Conference Series: Materials Science and Engineering 26, 2011.
[9] Edwards, P., O'Conner, A., Ramulu, M., "Electron Beam Additive Manufacturing of Titanium Components: Properties and Performance," Journal of Manufacturing Science and Engineering, Vol. 35, No. 24, Dec. 2013.
[10] Rafi, K. H., Karthik, N.V., Starr, Thomas L., Stucker, Brent E. "Mechanical property evaluation of Ti-6Al-4V parts made using Electron Beam Melting," Solid Freeform Fabrication Symposium, SFF23, Laboratroy for Freeform Fabrication at The University of Texas at Austin, 2012.

[11] Sterling, A. J., Torries, B., Shamsaei, N., Thompson, S. M., and Seely, D., and "Effects of Manufacturing Defects on Fatigue Behavior of Direct Laser Deposited Ti-6Al-4V," submitted.
[12] SAE AMS 4998C EN - Titanium Alloy Powder 6Al-4V-UNS R56400
[13] ASTM E 606-92 - Standard Practice for Strain-Controlled Fatigue Testing
[14] Nalla, R. K., Boyce, B. L., Campbell, J. P., Peters, J. O., and Ritchie, R. O., "Influence of Microstructure on High-Cycle Fatigue of Ti-6Al-4V: Bimodal vs. Lamellar Structures," Metallurgical and Materials Transactions, Vol. 33A, No. 13, 2002, pp. 899-918.